

Single-particle excitations in the uniform electron gas by diagrammatic Monte Carlo

Kristjan Haule^{1*} and Kun Chen²

¹*Department of Physics and Astronomy, Rutgers University, Piscataway, New Jersey 08854, USA and*

²*Center for Computational Quantum Physics, Flatiron Institute, 162 5th Avenue, New York, NY 10010. The Flatiron Institute is a division of the Simons Foundation*

(Dated: August 11, 2022)

We calculate the single-particle excitation spectrum and the Landau Fermi liquid parameters for the three-dimensional uniform electron gas with a numerically exact variational diagrammatic Monte Carlo method. In the metallic range of density, we establish benchmark values for the wave-function renormalization factor Z , the effective mass m^*/m , and the Landau parameters F_0^s and F_0^a with unprecedented accuracy, and we resolve the long-standing puzzle of non-monotonic dependence of mass on density. We also exclude the possibility that experimentally measured large reduction of bandwidth in Na metal can originate from the charge and spin fluctuations contained in the model of the uniform electron gas.

Introduction: The uniform electron gas (UEG) is the most fundamental model for understanding the electronic properties of metallic materials. The ground-state properties of the model have been very precisely calculated by quantum Monte Carlo methods [1], and this allowed one to build approximate density functionals [2, 3], which are at the heart of the ab-initio approaches in material science and modern theory-driven materials design. The knowledge of the low energy excitations of the same model remain challenging to evaluate accurately [4–10], even though such calculations are important for building more sophisticated density functionals [11–13], and these excitations are directly measured in experiments on simple metals, such as alkaline materials.

In the metallic regime, the low-energy properties of the electron liquid are dominated by the long-lived quasiparticles near the Fermi surface, and their dynamics is described by a handful of the Fermi liquid parameters. These parameters completely characterize the low energy excitation spectra of the metallic state. Unfortunately, they are very challenging to calculate by a first principle approach, therefore they are usually treated as phenomenological parameters requiring input from experiments.

Here we develop an extension of the recently introduced variational diagrammatic Monte Carlo (VDMC) method [14], which fills this void, and allows us to determine the single-particle excitations of UEG with unprecedented accuracy. In this letter, we calculate the single-particle excitation spectra, and in particular, we give controlled values of the wave-function renormalization factor Z , the quasiparticle effective mass ratio m^*/m and also the Landau Fermi liquid parameters F_0^a and F_0^s . Our computed values are free of systematic error, and their uncertainty is mainly controlled by the statistical error, and hence our established value can be used as a precise benchmark for new method development. Moreover, these precise Fermi liquid parameters are also useful

for building more sophisticated density functionals. Finally, the method we develop here can be used to solve more sophisticated models, and can also be used in the ab-initio framework on models of realistic materials, a development which is currently underway [15].

The VDMC method [14] is a flavor of diagrammatic Monte Carlo method (DMC) [16–23], which samples high-order Feynman diagrams with a Monte Carlo importance sampling. The novelty of VDMC is two-fold: i) it optimizes the starting point of the perturbative expansion in such a way that the expansion converges very rapidly with the increasing perturbation order. ii) it efficiently combines a large number of Feynman diagrams, which largely cancel among themselves due to alternating fermionic sign so that the groups of diagrams can be efficiently sampled with the Monte Carlo importance sampling hence avoiding the explosion of statistical error with perturbative order.

In Ref. 14 we computed the spin and the charge response functions of the UEG model with VDMC by evaluating the Feynman diagrams for the polarization function. A similar type of Feynman expansion in terms of non-interacting single-particle Green's function, and statically screened Coulomb interaction does not converge rapidly enough to establish a reliable infinite order result, hence we develop an alternative approach. In this work, we show that when using a Hedin-type equation, in which we first compute the numerically exact screened interaction $W_{\mathbf{q}}$ with previously developed VDMC, and we then expand the three-point vertex function Γ_3 in powers of statically screened interaction $v_{\mathbf{q}}$ and the bare electron propagator $G_{\mathbf{k}}^0$, with proper counter terms defined below, we can achieve very rapid convergence with the perturbative order. Fig. 1 shows the sketch of the corresponding Feynman diagrams up to the third order. To properly define the quantities entering the expansion, and in particular to evaluate the proper counter-terms of the expansion, we develop and test the theory on the UEG model, although the method is completely general and could as well be carried out for realistic material in the ab-initio framework.

*Electronic address: haule@physics.rutgers.edu

The Hamiltonian of UEG problem is

$$\hat{H} = \sum_{\mathbf{k}\sigma} (\mathbf{k}^2 - \mu) \hat{\psi}_{\mathbf{k}\sigma}^\dagger \hat{\psi}_{\mathbf{k}\sigma} + \frac{1}{2V} \sum_{\substack{\mathbf{q} \neq 0 \\ \mathbf{k}\mathbf{k}'\sigma\sigma'}} \frac{8\pi}{q^2} \hat{\psi}_{\mathbf{k}+\mathbf{q}\sigma}^\dagger \hat{\psi}_{\mathbf{k}'-\mathbf{q}\sigma'}^\dagger \hat{\psi}_{\mathbf{k}'\sigma'} \hat{\psi}_{\mathbf{k}\sigma}, \quad (1)$$

where $\hat{\psi}/\hat{\psi}^\dagger$ are the annihilation/creation operator of an electron, μ is the chemical potential controlling the density of the electrons in the system, and the long-range Coulomb repulsion is $8\pi/q^2$, as we measure the energy in units of Rydbergs, and the wave number k, q in units of inverse Bohr radius.

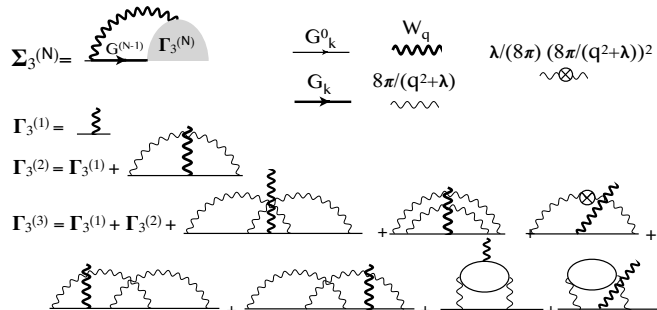


FIG. 1: **Feynman diagrams** for the self-energy in terms of the three leg vertex Γ_3 , which is expanded in bare series in terms of $G_{\mathbf{k}}^0$ and partially screened interaction $v_{\mathbf{q}} = \frac{8\pi}{q^2 + \lambda}$ and counter-terms $(\frac{\lambda}{8\pi})^N (\frac{8\pi}{q^2 + \lambda})^{N+1}$.

The expansion in terms of the bare interaction is divergent, therefore we first transform the original problem into an equivalent but a more appropriate problem for power expansion, which describes the emergent degrees of freedom at the lowest order, and the corrections are perturbatively included with very rapid convergence. Motivated by the well-known fact that the long-range Coulomb interaction is screened in the solid and that the effective potential of emerging quasiparticles differs from the bare potential, we introduce the screening parameter $\lambda_{\mathbf{q}}$ and an electron potential $v_{\mathbf{k}}$ into the quadratic part of the emergent Lagrangian L_0 of the form

$$L_0 = \sum_{\mathbf{k}\sigma} \psi_{\mathbf{k}\sigma}^\dagger \left(\frac{\partial}{\partial \tau} - \mu + \mathbf{k}^2 + v_{\mathbf{k}}(\xi = 1) \right) \psi_{\mathbf{k}\sigma} + \sum_{\mathbf{q} \neq 0} \phi_{-\mathbf{q}} \frac{q^2 + \lambda_{\mathbf{q}}}{8\pi} \phi_{\mathbf{q}}. \quad (2)$$

We then add the following interacting part to the Lagrangian

$$\Delta L = - \sum_{\mathbf{k}\sigma} \psi_{\mathbf{k}\sigma}^\dagger v_{\mathbf{k}}(\xi) \psi_{\mathbf{k}\sigma} - \xi \sum_{\mathbf{q} \neq 0} \phi_{-\mathbf{q}} \frac{\lambda_{\mathbf{q}}}{8\pi} \phi_{\mathbf{q}} + \sqrt{\xi} \frac{i}{\sqrt{2V}} \sum_{\mathbf{q} \neq 0} (\phi_{\mathbf{q}} \rho_{-\mathbf{q}} + \rho_{\mathbf{q}} \phi_{-\mathbf{q}}). \quad (3)$$

so that, when the number ξ is set to unity, $L(\xi) = L_0(\xi) + \Delta L(\xi)$ is Lagrangian of UEG. Indeed integrating out the bosonic fields $\phi_{\mathbf{q}}$ from Lagrangian L , we get the Lagrangian corresponding to the original Hamiltonian Eq. 1. Here $\rho_{\mathbf{q}}$ is the density fluctuation of the problem $\rho_{\mathbf{q}} = \sum_{\mathbf{k}\sigma} \psi_{\mathbf{k}\sigma}^\dagger \psi_{\mathbf{k}+\mathbf{q}\sigma}$. Note that the first two terms in ΔL are the counterterms [24] which exactly cancel the two terms we added to L_0 above. We use the number ξ to track the order of the Feynman diagrams so that order N contribution sums up all diagrams carrying the factor ξ^N . We set $\xi = 1$ once we enumerate all the diagrams of a certain order.

The emergent screening length $\lambda_{\mathbf{q}}$ and effective potential $v_{\mathbf{k}}$ are not a-priori known and need to be properly optimized to achieve an optimal speed of convergence. We note in passing that determining those parameters self-consistently, i.e., $\lambda_{\mathbf{q}}$ from the self-consistent polarization, and $v_{\mathbf{k}}$ from the single-particle self-energy, is not the most optimal choice for the speed of convergence. Determining them by the principal of minimal sensitivity is a much better choice, as pointed out by Kleinert and Feynman [25–28]. They showed that when an effective parameter of a theory is optimized with this principle, the perturbative expansion converges very fast, and can succeed even when the interaction is strong, and regular perturbation theory fails.

To make optimization manageable, we take $\lambda_{\mathbf{q}}$ to be \mathbf{q} independent constant (λ), and we will show that such a simple ansatz is already sufficient for rapid convergence. We emphasize that for any choice of these parameters we are guaranteed to converge to the same answer, provided that the series converges. Furthermore, we found that the convergence of the expansion is best when the Fermi surface of both the dressed $G_{\mathbf{k}}$ and the bare $G_{\mathbf{k}}^0$ Green's function at each order is fixed with the Luttinger's theorem so that the density and the Fermi surface volume is not changed with the increasing perturbation order. We therefore, expand $v_{\mathbf{k}}$ in power series $v_{\mathbf{k}} = (\Sigma_{\mathbf{k}}^x(\lambda) - \Sigma_{k_F}^x(\lambda)) + \xi s_1 + \xi^2 s_2 \dots$, and we determine s_N so that all contributions at the order ξ^N do not alter the physical volume of the Fermi surface. Similarly to optimizing $\lambda_{\mathbf{q}}$, we found that it is sufficient to take s_N constants independent of the momentum. Since the exchange ($\Sigma_{\mathbf{k}}^x$) is static and is typically large, we accommodate it at the zeroth-order into the effective potential, so that at the first order we recover the GW type self-energy with $G_{\mathbf{k}}$ at the screened Hartree-Fock (screened by screening length λ) and exact $W_{\mathbf{q}}$.

As mentioned before, the algorithm depicted in Fig. 1 needs a numerically exact (converged) $W_{\mathbf{q}}$, which is first computed with the algorithm of Ref. 14. It was shown in Ref. 14 that the most rapidly converging scheme for charge and spin-susceptibilities is the so-called vertex correction scheme, in which we add an infinite sum of ladder diagrams on both sides of a polarization Feynman diagram. To do that, we first precompute the three-point ladder vertex and then attach it to both sides of a polarization Feynman diagram while the diagrams are sam-

r_s	Z	m^*/m	F_0^a	F_0^s
1	0.8725(2)	0.955(1)	-0.171(1)	-0.209(5)
2	0.7984(2)	0.943(3)	-0.271(2)	-0.39(1)
3	0.7219(2)	0.965(3)	-0.329(3)	-0.56(1)
4	0.6571(2)	0.996(3)	-0.368(4)	-0.83(2)

TABLE I: VDMC computed values of the wave-function renormalization factor Z , effective mass m^*/m , and the Landau parameters F_0^a , F_0^s for various values of the density parameter r_s , together with the estimated error.

pled, and at the same time, we eliminate all ladder-type diagrams from the sampling, to avoid double-counting of diagrams. Next, we use Hedin's type equation depicted in Fig. 1 in which one fermion propagator is dressed and requires self-consistent G . It is easy to see that it is sufficient to use bold G of the lower order $N - 1$ when evaluating self-energy at order N , to avoid the expensive self-consistent calculation. Finally, we use the finite temperature imaginary-time formalism, and we set the temperature to $T = 0.04 E_F$, which is sufficiently below the Fermi liquid scale, so that is essentially equivalent to zero temperature.

Results: We first present the single-particle excitation spectral results of this rapidly converging algorithm described above. Fig. 2a-c shows how the wave-function renormalization factor Z depends on the screening parameter λ in our theory. To determine the optimized parameter λ , we scan $Z(\lambda)$ for each r_s , and determine it with the principle of minimal sensitivity. For efficiency, we here sample the self-energy only at the Fermi wave vector k_F and at the two lowest Matsubara frequencies, which is sufficient to determine Z . We notice that for the first two orders, no counter term in the parameter λ occurs, therefore the curve $Z(\lambda)$ displayed in Fig. 2 does not have extremum, while all higher-order terms have a well-defined maximum, which broadens and develops into a broad plateau with increasing order. The insets of Figs. 2a-c show optimized Z versus perturbation order, where the first two orders are evaluated at the optimal λ of the third order, and for later orders, we take the value in the maximum. We also display the value of λ used at each order. From Fig. 2 it is apparent that beyond order three the rate of convergence to limiting value of Z is extremely fast, and therefore we can confidently determine the first three digits of Z . The values and the estimated error-bar from the extrapolation and statistical errors are shown in Table I.

In Fig. 2d we compare our computed $Z(r_s)$ with the previous best available estimates, obtained by various flavors of Monte Carlo (MC) methods. Note that all these published MC methods rely on fixed node approximation and the thermodynamic limit extrapolation, hence they have an inherent systematic error. Our current work based on VDMC has only statistical error, and a small error in extrapolating in perturbation order, and is thus far more precise than previous best results. We notice that

previous MC results are broadly consistent with our results, with SJ-VMC method predicting slightly too large and BF-VMC and BF-RMC slightly too small value. It is also well known that G0W0 predicts quite accurate Z values, however, we can now confidently claim that in the range of metallic densities, G0W0 consistently underestimates Z .

Once the extremal value of λ is determined, we compute the entire momentum and frequency dependence of the self-energy, which allows us to determine also the momentum derivative of the self-energy, and hence the effective mass of the electron through the relation

$$\frac{m}{m^*} = Z \left(1 + \frac{m}{k_F} \frac{d\Sigma(k_F, \omega = 0)}{dk} \right) \quad (4)$$

The convergence of the effective mass ratio m^*/m with perturbation order is shown in Fig. 3a, and its dependence on r_s is displayed in Fig. 3b.

The dependence of the effective mass m^*/m on r_s has been controversial for many decades. Some theories predict that the ratio is monotonically decreasing with increasing r_s [7, 30], while others predict the existence of a turning point r_s^* [29, 31–34] at which the trend is reversed. Our controlled results confirm the correctness of the later theories. Furthermore, we compare our controlled VDMC results with previous best estimates, which are based on the theory of many-body local field factors [29]. This theory includes vertex corrections associated with charge and spin fluctuations, extracted from available Monte Carlo data. We notice that G0W0 overestimates the effective mass in the entire range of metallic densities. The density fluctuations beyond RPA are included in theory with G_+ local field corrections, which reduce the mass substantially and bring it very close to our VDMC results at small r_s . However, beyond $r_s > 3$ our VDMC results are closer to the theory which contains both the charge and the spin fluctuations ($G_+ \& G_-$), hence we can infer that at moderate correlations strength, the spin fluctuations start to play an important role, and charge fluctuations are no longer sufficient in determining the mass of the electron gas.

With precisely calculated effective mass, as well as the spin and charge susceptibility determined in our previous work [14], we can calculate Landau parameters F_0^a and F_0^s , which are obtained from $\frac{\chi_s}{\chi_s^0} = \frac{m^*}{m} \frac{1}{1+F_0^a}$ and $\frac{P_{q=0}}{P_{q=0}^0} = \frac{m^*}{m} \frac{1}{1+F_0^s}$. Here χ_s and P_q are the spin susceptibility and charge polarization, while χ_s^0 and P_q^0 are their non-interacting analogues. In table I we list our calculated Landau parameters F_0^a and F_0^s , together with the estimation of their error, which mostly comes from error in determining spin and charge susceptibility in Ref. 14. While the Landau parameters, which determine the interaction between quasiparticle, have been estimated by various approximate numerical methods before [7], to our knowledge their numerically controlled value has not been obtained before.

The present VDMC algorithm allows us to compute a

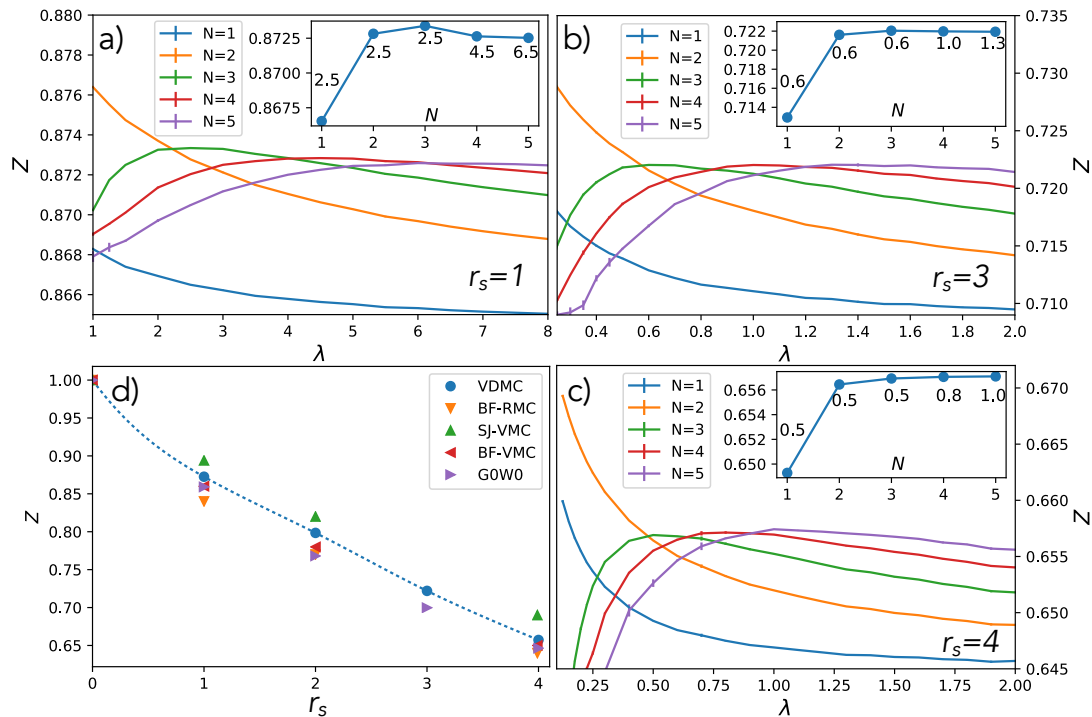


FIG. 2: **wave-function renormalization factor** Z versus screening parameter λ for various perturbation orders $N = 1 \dots 5$ and for $r_s = 1, 2, 3$ and 4 . The insets show the convergence of Z with perturbation order N when its value is taken at the extremal λ . The numbers next to each point show the value of λ used for each calculated point.

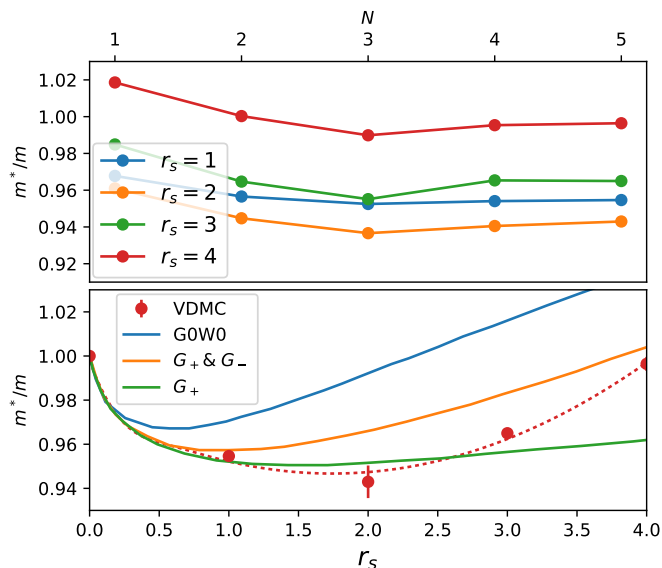


FIG. 3: **Electron effective mass:** The upper panel shows our calculated effective mass versus perturbation order for $r_s = 1 - 4$. The lower panel compares the r_s dependence of the effective mass of this work (VDMC) with the prior analytic and numeric work from Ref. 29.

numerically controlled value for the dynamic self-energy on the imaginary axis. Analytic continuation is needed to obtain the self-energy on the real frequency axis. We

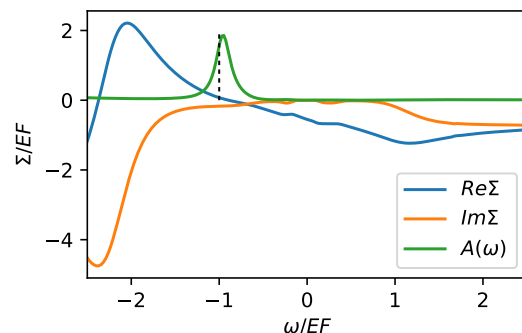


FIG. 4: **The spectral function** and $\Sigma_{k=0}(\omega)$ at $r_s = 4$ and $k = 0$ as relevant for bandwidth of Na metal.

use the maximum entropy method to compute the quasi-particle energy at the $k = 0$ point, which determines the bandwidth of the electron dispersion, i.e., the energy difference between the Fermi level and the lowest possible quasi-particle energy. In Fig. 4 we display the self-energy, as well as the spectral function at momentum $k = 0$ and finite frequency. We notice that the imaginary part of the self-energy starts to grow rapidly when the energy of the single-particle excitations exceeds the plasma frequency $\omega_p \approx 1.881E_F$. Consequently, there appears a strong pole at $\omega \approx -2.4E_F$ due to such plasma excitations, and makes quasi-particle approximation invalid at a frequency below $\omega < -E_F$, as the real part of the self-

energy is no longer a linear function of frequency. However, around E_F the real-part of Σ is still quite close to a linear function, and only minor deviations are noticed. Consequently, the renormalization of the dispersion can not substantially deviate from our earlier estimation of m^*/m , which is valid at the Fermi level. Our numerical estimation based on the analytically continued self-energy is that the spectral function at $r_s = 4$ and $k = 0$ has a peak around $-0.96E_F$, which deviates from the non-interacting value for only 4%, hence the bandwidth reduction due to interactions at $r_s = 4$ is only of the order of 4%. This value is much smaller than the experimental estimation of the bandwidth reduction in Na metal, in which the measured ARPES bandwidth appears to be renormalized for about 18-25% [35, 36]. However, our estimated bandwidth is definitely not substantially larger as compared to the non-interacting bandwidth, in contrast to several other many-body calculations [37, 38], and is neither substantially smaller as in early GW calculations [39] or GW with paramagnon vertex corrections [8]. Based on our very precise estimation of the single-particle self-energy, we can confidently exclude a

possibility of such a dramatic reduction of the bandwidth in the model of electron gas due to correlation effects at the density corresponding to Na metal. This large reduction of the effective mass in ARPES thus requires an alternative explanation, which was assigned to the interaction in the final states [38, 40] in ARPES, surface effects [41], and possibly the lattice effects, i.e. deviation of Na metal from the continuous model of the uniform electron gas.

In summary, we established the low energy excitation spectrum of the uniform electron gas at metallic density using recently developed VDMC. Controlled values of Z , m^*/m , F_0^s , and F_0^a are given, which agree with the state of the art calculations in the field, but here we provide much more precise values than previously known.

Acknowledgments: We thank N. Prokof'ev and B. Svistunov for stimulating discussion. This work was supported by the Simons Collaboration on the Many Electron Problem. KH acknowledges supported of NSF DMR-1709229. The Flatiron Institute is a division of the Simons Foundation.

-
- [1] Ceperley, D. M. & Alder, B. J. Ground state of the electron gas by a stochastic method. *Phys. Rev. Lett.* **45**, 566–569 (1980). URL <https://link.aps.org/doi/10.1103/PhysRevLett.45.566>.
- [2] Jones, R. O. & Gunnarsson, O. The density functional formalism, its applications and prospects. *Rev. Mod. Phys.* **61**, 689–746 (1989). URL <https://link.aps.org/doi/10.1103/RevModPhys.61.689>.
- [3] Perdew, J. P., Burke, K. & Ernzerhof, M. Generalized gradient approximation made simple. *Phys. Rev. Lett.* **77**, 3865–3868 (1996). URL <https://link.aps.org/doi/10.1103/PhysRevLett.77.3865>.
- [4] Simon, G. E. & Giuliani, G. F. Many-body local fields theory of quasiparticle properties in a three-dimensional electron liquid. *Physical Review B* **77**, 035131 (2008).
- [5] Takada, Y. Inclusion of vertex corrections in the self-consistent calculation of quasiparticles in metals. *Phys. Rev. Lett.* **87**, 226402 (2001). URL <https://link.aps.org/doi/10.1103/PhysRevLett.87.226402>.
- [6] Yasuhara, H., Yoshinaga, S. & Higuchi, M. Why is the bandwidth of sodium observed to be narrower in photoemission experiments? *Phys. Rev. Lett.* **83**, 3250–3253 (1999). URL <https://link.aps.org/doi/10.1103/PhysRevLett.83.3250>.
- [7] Yasuhara, H. & Ousaka, Y. Effective mass, Landau interaction function and self-energy of an electron liquid. *International Journal of Modern Physics B* **06**, 3089–3145 (1992). URL <https://doi.org/10.1142/S0217979292002401>. <https://doi.org/10.1142/S0217979292002401>.
- [8] Zhu, X. & Overhauser, A. W. Plasmon-pole and paramagnon-pole model of an electron liquid. *Phys. Rev. B* **33**, 925–936 (1986). URL <https://link.aps.org/doi/10.1103/PhysRevB.33.925>.
- [9] Richardson, C. F. & Ashcroft, N. W. Dynamical local-field factors and effective interactions in the three-dimensional electron liquid. *Phys. Rev. B* **50**, 8170–8181 (1994). URL <https://link.aps.org/doi/10.1103/PhysRevB.50.8170>.
- [10] Kukkonen, C. A. & Overhauser, A. W. Electron-electron interaction in simple metals. *Phys. Rev. B* **20**, 550–557 (1979). URL <https://link.aps.org/doi/10.1103/PhysRevB.20.550>.
- [11] Perdew, J. P., Kurth, S., Zupan, A. c. v. & Blaha, P. Accurate density functional with correct formal properties: A step beyond the generalized gradient approximation. *Phys. Rev. Lett.* **82**, 2544–2547 (1999). URL <https://link.aps.org/doi/10.1103/PhysRevLett.82.2544>.
- [12] Tran, F. & Blaha, P. Accurate band gaps of semiconductors and insulators with a semilocal exchange-correlation potential. *Phys. Rev. Lett.* **102**, 226401 (2009). URL <https://link.aps.org/doi/10.1103/PhysRevLett.102.226401>.
- [13] Sun, J., Ruzsinszky, A. & Perdew, J. P. Strongly constrained and appropriately normed semilocal density functional. *Phys. Rev. Lett.* **115**, 036402 (2015). URL <https://link.aps.org/doi/10.1103/PhysRevLett.115.036402>.
- [14] Chen, K. & Haule, K. A combined variational and diagrammatic quantum Monte Carlo approach to the many-electron problem. *Nature Communications* **10**, 3725 (2019). URL <https://doi.org/10.1038/s41467-019-11708-6>.
- [15] Haule, K. & Mandal, S. All electron gw with linearized augmented plane waves for metals and semiconductors. *arXiv preprint arXiv:2008.07727* (2020).
- [16] Prokof'ev, N. V. & Svistunov, B. V. Polaron problem by diagrammatic quantum monte carlo. *Physical review letters* **81**, 2514 (1998).
- [17] Prokof'ev, N. & Svistunov, B. Fermi-polaron problem:

- Diagrammatic monte carlo method for divergent sign-alternating series. *Physical Review B* **77**, 020408 (2008).
- [18] Van Houcke, K. *et al.* Feynman diagrams versus fermi-gas feynman emulator. *Nature Physics* **8**, 366 (2012).
- [19] Houcke, K. V., Kozik, E., Prokof'ev, N. & Svistunov, B. Diagrammatic monte carlo. *Physics Procedia* **6**, 95 – 105 (2010). Computer Simulations Studies in Condensed Matter Physics XXI.
- [20] Kozik, E. *et al.* Diagrammatic monte carlo for correlated fermions. *EPL (Europhysics Letters)* **90**, 10004 (2010).
- [21] Deng, Y., Kozik, E., Prokof'ev, N. V. & Svistunov, B. V. Emergent bcs regime of the two-dimensional fermionic hubbard model: Ground-state phase diagram. *EPL (Europhysics Letters)* **110**, 57001 (2015).
- [22] Rossi, R. Determinant diagrammatic monte carlo algorithm in the thermodynamic limit. *Phys. Rev. Lett.* **119**, 045701 (2017). URL <https://link.aps.org/doi/10.1103/PhysRevLett.119.045701>.
- [23] Rossi, R., Ohgoe, T., Van Houcke, K. & Werner, F. Resummation of diagrammatic series with zero convergence radius for strongly correlated fermions. *arXiv preprint arXiv:1802.07717* (2018).
- [24] Wu, W., Ferrero, M., Georges, A. & Kozik, E. Controlling feynman diagrammatic expansions: Physical nature of the pseudogap in the two-dimensional hubbard model. *Phys. Rev. B* **96**, 041105 (2017).
- [25] Stevenson, P. M. Gaussian effective potential: Quantum mechanics. *Physical Review D* **30**, 1712 (1984).
- [26] Stevenson, P. M. Gaussian effective potential. ii. $\lambda \varphi^4$ field theory. *Physical Review D* **32**, 1389 (1985).
- [27] Stevenson, P. M. & Tarrach, R. The return of $\lambda\varphi^4$. *Physics Letters B* **176**, 436–440 (1986).
- [28] Kleinert, H. *Path integrals in quantum mechanics statistics and polymer physics* (World Scientific, 1995).
- [29] Simion, G. E. & Giuliani, G. F. Many-body local fields theory of quasiparticle properties in a three-dimensional electron liquid. *Phys. Rev. B* **77**, 035131 (2008). URL <https://link.aps.org/doi/10.1103/PhysRevB.77.035131>.
- [30] Lam, J. Thermodynamic properties of the electron gas at metallic densities. *Phys. Rev. B* **5**, 1254–1260 (1972). URL <https://link.aps.org/doi/10.1103/PhysRevB.5.1254>.
- [31] Hubbard, J. The description of collective motions in terms of many-body perturbation theory. *Proc. R. Soc. Lond. A* **240**, 539–560 (1957).
- [32] Rice, T. The effects of electron-electron interaction on the properties of metals. *Annals of Physics* **31**, 100 – 129 (1965). URL <http://www.sciencedirect.com/science/article/pii/0003491665902344>.
- [33] Hedin, L. & Lundqvist, S. Effects of electron-electron and electron-phonon interactions on the one-electron states of solids. vol. 23 of *Solid State Physics*, 1 – 181 (Academic Press, 1970). URL <http://www.sciencedirect.com/science/article/pii/S0081194708606153>.
- [34] MacDonald, A. H., Dharma-wardana, M. W. C. & Geldart, D. J. W. Density functional approximation for the quasiparticle properties of simple metals. i. theory and electron gas calculations. *Journal of Physics F: Metal Physics* **10**, 1719–1736 (1980). URL <https://doi.org/10.1088/2F0305-4608%2F10%2F8%2F010>.
- [35] Jensen, E. & Plummer, E. W. Experimental band structure of na. *Phys. Rev. Lett.* **55**, 1912–1915 (1985). URL <https://link.aps.org/doi/10.1103/PhysRevLett.55.1912>.
- [36] Lyo, I.-W. & Plummer, E. W. Quasiparticle band structure of na and simple metals. *Phys. Rev. Lett.* **60**, 1558–1561 (1988). URL <https://link.aps.org/doi/10.1103/PhysRevLett.60.1558>.
- [37] Maezono, R., Towler, M. D., Lee, Y. & Needs, R. J. Quantum monte carlo study of sodium. *Phys. Rev. B* **68**, 165103 (2003). URL <https://link.aps.org/doi/10.1103/PhysRevB.68.165103>.
- [38] Takada, Y. Inclusion of vertex corrections in the self-consistent calculation of quasiparticles in metals. *Phys. Rev. Lett.* **87**, 226402 (2001). URL <https://link.aps.org/doi/10.1103/PhysRevLett.87.226402>.
- [39] Northrup, J. E., Hybertsen, M. S. & Louie, S. G. Theory of quasiparticle energies in alkali metals. *Phys. Rev. Lett.* **59**, 819–822 (1987). URL <https://link.aps.org/doi/10.1103/PhysRevLett.59.819>.
- [40] Shung, K. W. K. & Mahan, G. D. Calculated photoemission spectra of na. *Phys. Rev. Lett.* **57**, 1076–1079 (1986). URL <https://link.aps.org/doi/10.1103/PhysRevLett.57.1076>.
- [41] Shung, K. W. K., Sernelius, B. E. & Mahan, G. D. Self-energy corrections in photoemission of na. *Phys. Rev. B* **36**, 4499–4502 (1987). URL <https://link.aps.org/doi/10.1103/PhysRevB.36.4499>.